JPE 14-5-8

http://dx.doi.org/10.6113/JPE.2014.14.5.874
ISSN(Print): 1598-2092 / ISSN(Online): 2093-4718

Analysis and Design of a PFC AC–DC Converter with Electrical Isolation

Chia-Ching Lin[*], Lung-Sheng Yang[†], and Ren-Jun Zheng[*]

[*†]Department of Electrical Engineering, Far East University, Tainan City, Taiwan

Abstract

This study presents a single-phase power factor correction AC–DC converter that operates in discontinuous conduction mode. This converter uses the pulse-width modulation technique to achieve almost unity power factor and low total harmonic distortion of input current for universal input voltage (90 V_{rms} to 264 V_{rms}) applications. The converter has a simple structure and electrical isolation. The magnetizing-inductor energy of the transformer can be recycled to the output without an additional third winding. The steady-state analysis of voltage gain and boundary operating conditions are discussed in detail. Finally, experimental results are shown to verify the performance of the proposed converter.

Key words: DCM, PFC, PWM, THD_i

I. INTRODUCTION

DC power sources are widely used in industrial products and consumer electronics, such as battery chargers, DC power supplies, uninterruptible power supplies, inverters, and instruments. Thus, AC–DC power conversion is an important consideration. Diode-bridge or thyristor rectifiers can realize AC–DC power conversion, but such rectifiers will result in power pollution, including pulsating input current, low power factor, and high total harmonic distortion of input current (THD_i). Several power factor correction (PFC) AC–DC converters have been investigated to address these issues. These converters possess non-isolated and isolated topologies. Non-isolated topologies include the boost [1]-[4], buck [5]-[7], buck-boost [8]-[10], Cuk [11], SEPIC [12], [13], and ZETA types [14]. These converters are operated in continuous conduction mode and discontinuous conduction mode (DCM) for different output-power applications. Isolated topologies include forward [15]-[17] and flyback types [18]-[20]. The forward types achieve low output voltage ripple and high THD_i. Nevertheless, this converter requires the third winding to recycle the magnetizing-inductor energy of the transformer. The flyback types are shown in Fig. 1(a). This converter achieves high power factor and low THD_i. Moreover, flyback types have a simple structure and low cost but have low efficiency because of the transformer leakage inductor. The clamping method is presented in [21], [22] to recycle leakage inductor energy. However, this method makes the power circuit complicated.

We propose a single-phase PFC AC–DC converter, as shown in Fig. 1(b). The proposed converter circuit configuration is very simple. The configuration includes only a set of input filter L_f–C_f, a diode-bridge rectifier, a transformer T_r, an inductor L_1, an output diode D_o, and an output capacitor C_o. The proposed converter does not have the transformer leakage inductor issue associated with the flyback converter. Moreover, transformer magnetizing-inductor energy can be recycled to the output without an additional third winding. This converter is operated in DCM by using the pulse–width modulation technique to achieve high power factor and low THD_i for universal input-voltage applications.

II. OPERATING PRINCIPLES

The equivalent circuit of the proposed converter is shown in Fig. 2. The transformer is modeled as a magnetizing inductor L_m and an ideal transformer. Some key waveforms in a half line-source period are shown in Fig. 3. The operating principle is analyzed as $0 < \omega t < \pi$, where ω is the line angular frequency, because of the symmetrical characteristics of the single-phase system.

Mode 1, $[kT_s, t_{k1}]$: S_1 is switched on. The current- flow path is shown in Fig. 4(a). The line source energy is transferred to the magnetizing inductor L_m of the transformer and the

Manuscript received Dec. 30, 2013; accepted May 3, 2014
Recommended for publication by Associate Editor Joung-Hu Park.
[†]Corresponding Author: yanglungsheng@yahoo.com.tw
Tel: +886-6-5979566-5410, Far East University
[*]Dept. of Electric Eng., Far East University, Taiwan

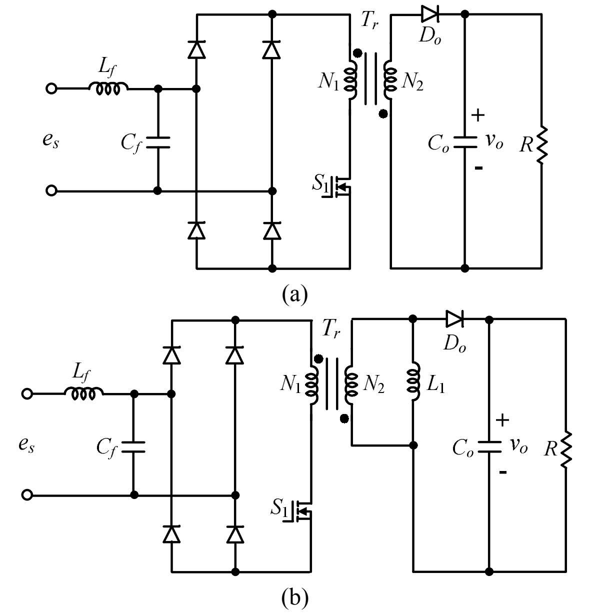

Fig. 1. (a) Conventional single-phase AC–DC flyback converter and (b) proposed single-phase AC–DC converter.

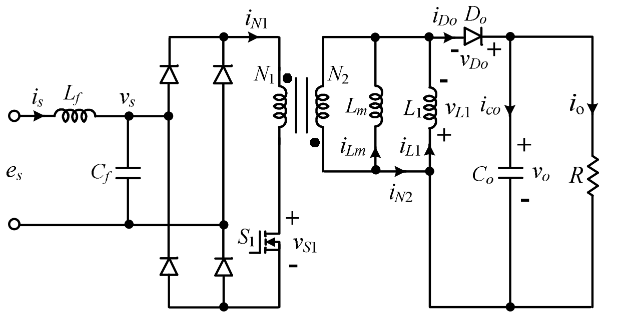

Fig. 2. Equivalent circuit of proposed converter.

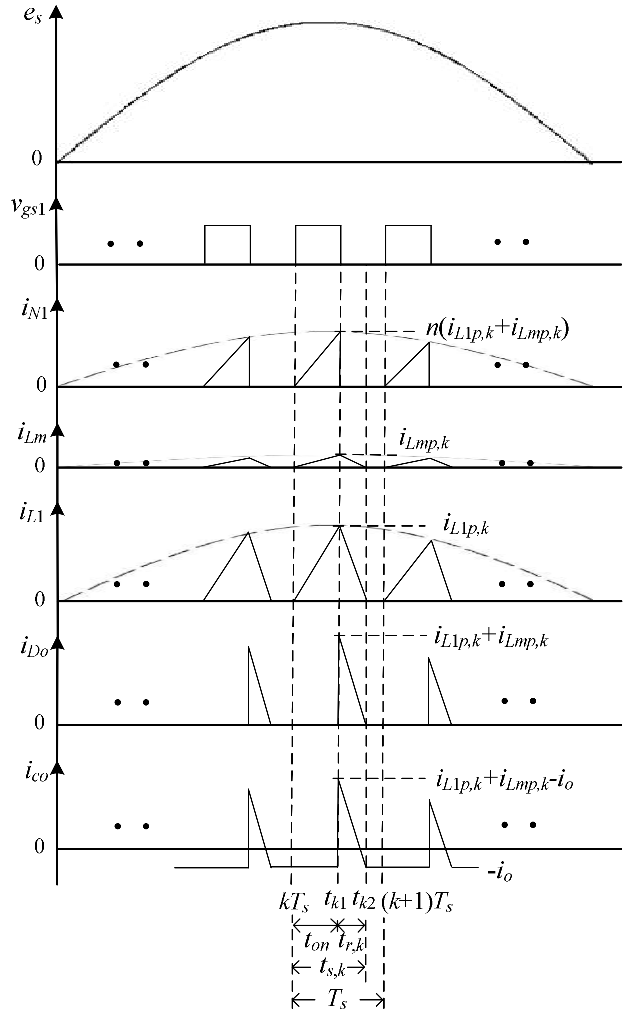

Fig. 3. Key waveforms of the proposed converter for $0<\omega t<\pi$.

inductor L_1. Thus, the currents i_{Lm} and i_{L1} are increased linearly. Given that magnetizing inductor L_m is significantly larger than inductor L_1, the magnetizing-inductor current i_{Lm} becomes lower than inductor current i_{L1}. The energy stored in magnetizing inductor L_m is the residual magnetism of the transformer. The energy stored in output capacitor C_o is discharged to load R. This mode ends when S_1 is switched off.

Mode 2, $[t_{k1}, t_{k2}]$: S_1 is switched off. The current-flow path is shown in Fig. 4(b). The energies stored in magnetizing inductor L_m and inductor L_1 are released to output capacitor C_o and load R. The currents i_{Lm} and i_{L1} are decreased linearly. This mode ends when the currents i_{Lm} and i_{L1} are equal to zero. Therefore, the transformer residual magnetism can be released to empty during each switching period.

Mode 3, $[t_{k2}, (k+1)T_s]$: S_1 remains switched off. The current-flow path is shown in Fig. 4(c). The energies stored in magnetizing inductor L_m and inductor L_1 are empty at $t = t_{k2}$. The energy stored in output capacitor C_o is discharged to load R. This mode ends when S_1 is switched on at the beginning of the next switching period.

III. Steady-State Analysis

Given that the single-phase system is symmetrical, the following analysis is discussed for $0 < \omega t < \pi$. For simplicity, the effect of the input filter is neglected. The line voltage is given by

$$e_s(t) = v_s(t) = \sqrt{2}V_{rms}\sin\omega t = V_m \sin\omega t \tag{1}$$

where V_{rms} and V_m are the root-mean-square value and line voltage amplitude, respectively. The line voltage is considered a piecewise constant during each switching period because switching frequency f_s is larger than line frequency f_1. If m is the switching number within $[0, \pi/\omega]$, then m is equal to $f_s/2f_1$. The following analysis is considered during switching period $[kT_s, (k+1)T_s]$, where $k = 0, 1, \ldots, m-1$. The magnetizing inductor L_m is ignored in the following analysis because it is significantly larger than inductor L_1.

When S_1 switched turned on, the voltage across inductor L_1 is obtained as

$$v_{L1} = n \times |e_s(t_k)| \tag{2}$$

where es(tk) is the input-voltage level during switching the

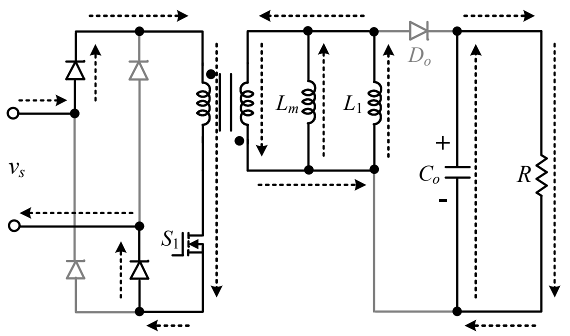

(a) Mode 1.

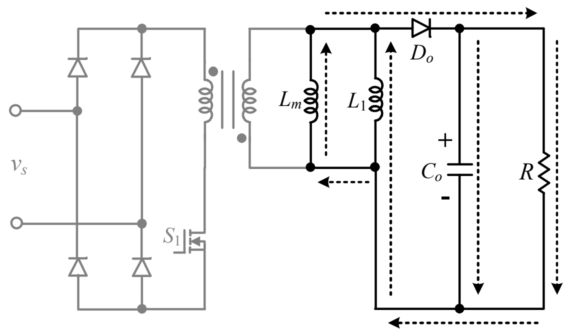

(b) Mode 2.

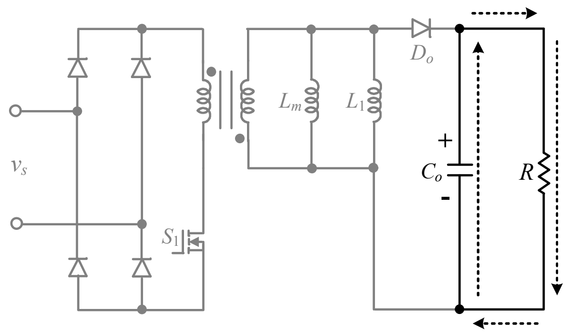

(c) Mode 3.

Fig. 4. Current flow path of the proposed converter for $0<\omega t<\pi$.

period $[kT_s, (k+1)T_s]$, and the turns ratio of transformer $n = N_2/N_1$. Then,

$$\frac{di_{L1}(t)}{dt} = \frac{n\times|e_s(t_k)|}{L_1}, \quad kT_s \le t \le t_{k1} \tag{3}$$

The inductor current i_{L1} is given by

$$i_{L1}(t) = \frac{n\times|e_s(t_k)|}{L_1}(t-kT_s), \quad kT_s \le t \le t_{k1} \tag{4}$$

When t is equal to t_{k1}, the peak value of inductor current i_{L1} is

$$i_{L1p,k} = \frac{n\times|e_s(t_k)|}{L_1}t_{on} = \frac{n\times|e_s(t_k)|}{L_1}dT_s \tag{5}$$

where $t_{on} = t_{k1} - kT_s = dT_s$.

When S_1 is switched off, the voltage across inductor L_1 is given by

$$v_{L1} = -v_o \tag{6}$$

Then,

$$\frac{di_{L1}(t)}{dt} = -\frac{v_o}{L_1} \tag{7}$$

By solving (7), we derive the inductor current i_{L1} as follows:

$$i_{L1}(t) = -\frac{v_o}{L_1}(t-t_{k1}) + i_{L1p,k}, \quad t_{k1} \le t \le t_{k2} \tag{8}$$

Given that $i_{L1}(t_{k2}) = 0$, the peak value of inductor current i_{L1} is

$$i_{L1p,k} = \frac{v_o}{L_1}t_{r,k} \tag{9}$$

where $t_{r,k} = t_{k2} - t_{k1}$.

Using (5) and (9), time duration $t_{r,k}$ can be given by

$$t_{r,k} = \frac{n\cdot|e_s(t_k)|}{v_o}dT_s \tag{10}$$

A. Power Factor Correction

As shown in Fig. 3, the average value of unfiltered input current i_{N1} in one switching period T_s can be computed as

$$i_{N1,avg}(t) = \frac{t_{on} n i_{L1p}}{2T_s} \tag{11}$$

where i_{L1p} is the inductor current peak value for each switching period. Substituting (1) and (5) into (11), we derive the following equation:

$$i_{N1,avg}(t) = \frac{t_{on} n i_{L1p}}{2T_s} = \frac{d^2 n^2 T_s V_m}{2L_1}|\sin\omega t| \tag{12}$$

The average value of unfiltered input current i_{N1} is sinusoidal and in phase with the input voltage. Moreover, the harmonic components of current i_{N1} are distributed over the switching frequency multiples. The harmonic components are easily filtered out by using input filter L_f–C_f. The input filter cutoff frequency is significantly lower than the switching frequency.

B. Voltage Gain

From Fig. 3, the average value of the output-capacitor current i_{co} during $[kT_s, (k+1)T_s]$ can be obtained as

$$i_{co,k(avg)} = \frac{\frac{1}{2}t_{r,k}i_{L1p,k} - i_oT_s}{T_s} \tag{13}$$

Substituting (1), (5), and (10) into (13) yields

$$i_{co,k(avg)} = \frac{n^2d^2V_m^2T_s}{2L_1v_o}\sin^2\omega t_k - \frac{v_o}{R} \tag{14}$$

The average value of output–capacitor current i_{co} during a half line-source period $[0, \pi/\omega]$ is written as follows:

$$i_{co,avg} = \frac{\omega}{\pi}\sum_{k=0}^{m-1} i_{co,k}T_s = \frac{\omega}{\pi}\sum_{k=0}^{m-1}\left(\frac{n^2d^2V_m^2T_s}{2L_1v_o}\sin^2\omega t_k - \frac{v_o}{R}\right)T_s \tag{15}$$

Given that m is larger than 1, equation (15) is approximated as:

$$i_{co,avg} = \frac{\omega}{\pi}\int_0^{\frac{\pi}{\omega}}\left(\frac{n^2d^2V_m^2T_s}{2L_1v_o}\sin^2\omega t - \frac{v_o}{R}\right)dt = \frac{n^2d^2V_m^2T_s}{4L_1v_o} - \frac{v_o}{R} \tag{16}$$

The output voltage differential equation is given by

$$\frac{d}{dt}v_o = \frac{1}{C_o}\left(\frac{n^2 d^2 V_m^2 T_s}{4L_1 v_o} - \frac{v_o}{R}\right) \tag{17}$$

The DC model equation is written as

$$\frac{n^2 D^2 V_m^2 T_s}{4L_1 V_o} = \frac{n^2 D^2 V_m^2}{4L_1 f_s V_o} = \frac{V_o}{R} \tag{18}$$

where V_o and D are the DC quantities of v_o and d, respectively.

The normalized inductor time constant is then defined as

$$\tau_{L1} \equiv \frac{L_1 f_s}{R} \tag{19}$$

Substituting (19) into (18), the voltage gain is derived as

$$M = \frac{V_o}{V_m} = \frac{nD}{2\sqrt{\tau_{L1}}} \tag{20}$$

C. Boundary Condition

The current i_{L1} must be zero in each switching period to ensure that the proposed converter is operated in DCM. From Fig. 3, time duration $t_{s,k}$ is obtained as

$$t_{s,k} = t_{on} + t_{r,k} = \frac{DT_s(V_o + n\cdot|e_s|)}{V_o} \tag{21}$$

When the maximum value of $t_{s,k}$ is equal to T_s and $|e_s|$ is equal to V_m, the proposed converter is operated in boundary conduction mode. Therefore, substituting $t_{s,k} = T_s$ and $|e_s| = V_m$ into (21) can determine the boundary voltage gain as

$$M_{bc} = \frac{V_o}{V_m} = \frac{nD}{1-D} \tag{22}$$

Using (20) and (22), the curves of voltage gain and boundary voltage gain are shown in Fig. 5. When the voltage gain M is equal to its boundary voltage gain M_{bc}, the boundary normalized inductor time constant τ_{L1B} is given by

$$\tau_{L1B} = \frac{(1-D)^2}{4} \tag{23}$$

τ_{L1B} is plotted in Fig. 6. We can observe that the proposed converter is operated in DCM when $\tau_{L1} < \tau_{L1B}$.

IV. Selections of Inductor and Capacitor

A. Selection of Inductor L_1

The appropriate τ_{L1B} is selected under the required voltage gain to ensure that the proposed converter is operated in DCM. The inductor L_1 needs to satisfy the following inequality:

$$L_1 < \frac{R}{f_s}\tau_{L1B} \tag{24}$$

B. Selection of Output Capacitor C_o

Using (14), the average value of output–capacitor current i_{co} during one switching period is simplified as follows:

$$i_{co,k} = \left(\frac{n^2 D^2 V_m^2}{4L_1 f_s V_o} - \frac{V_o}{R}\right) - \frac{n^2 D^2 V_m^2}{4L_1 f_s V_o}\cos 2\omega t_k \tag{25}$$

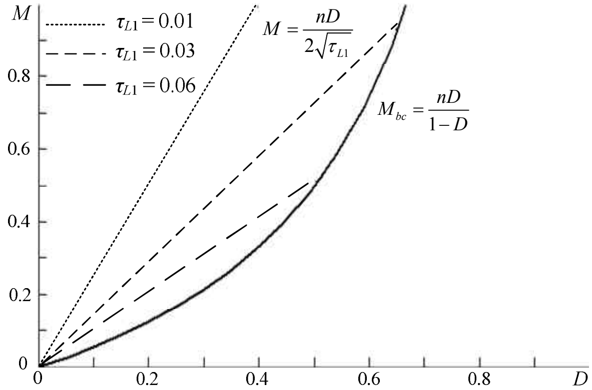

Fig. 5. Voltage gain and boundary voltage gain (under n = 0.5).

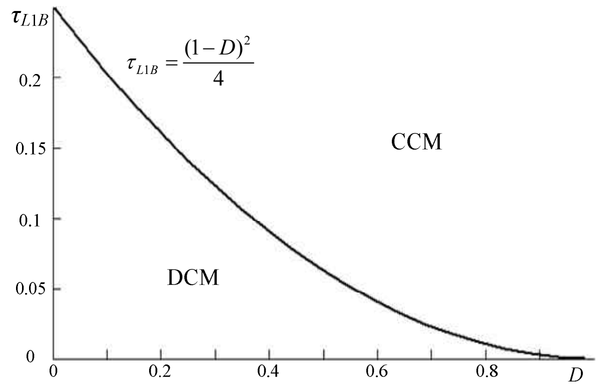

Fig. 6. Boundary operating condition.

Substituting (18) into (25), output–capacitor current i_{co} is expressed as

$$i_{co,k} = \frac{-n^2 D^2 V_m^2}{4L_1 f_s V_o}\cos 2\omega t_k \tag{26}$$

Therefore, the output voltage ripple in one switching period is given by

$$\Delta V_{o,k} = \left(\frac{-n^2 D^2 V_m^2}{4L_1 C_o f_s V_o}\cos 2\omega t_k\right)T_s \tag{27}$$

Then, the output voltage ripple function during time interval $[0, \pi/\omega]$ is obtained as

$$\Delta V_o(t) = \int_0^t \left(\frac{-n^2 D^2 V_m^2}{4L_1 C_o f_s V_o}\cos 2\omega t'\right)dt' = \frac{-n^2 D^2 V_m^2}{4L_1 C_o f_s V_o} \times \frac{\sin 2\omega t}{2\omega} \tag{28}$$

Using (28), the output voltage ripple during time interval $[0, \pi/\omega]$ is derived as

$$V_{o,ripple} = 2\left|\Delta V_o(t)\right|_{peak} = \frac{n^2 D^2 V_m^2}{4\omega L_1 C_o f_s V_o} \tag{29}$$

Thus,

$$\frac{V_{o,ripple}}{V_o} = \frac{n^2 D^2 V_m^2}{4\omega L_1 C_o f_s V_o^2} = \frac{n^2 D^2}{4\omega L_1 C_o f_s M^2} \tag{30}$$

Output capacitor C_o must satisfy the following inequality to meet the following output voltage ripple percentage specification:

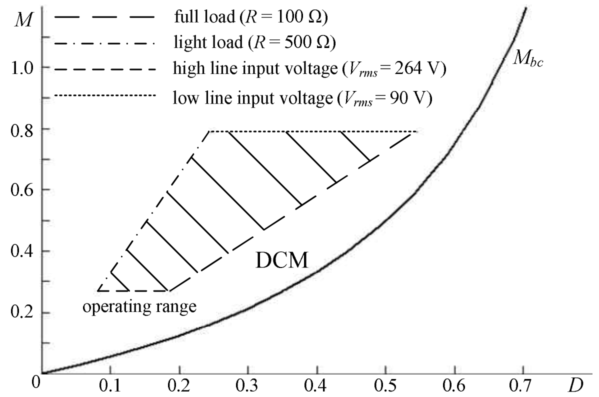

Fig. 7. Operating range of the prototype circuit.

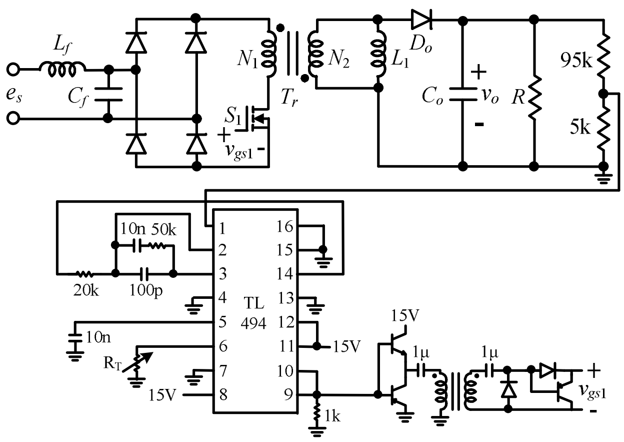

Fig. 8. Control circuit of the proposed converter.

$$C_o \geq \frac{n^2 D^2}{4\omega L_1 f_s M^2} \times \frac{V_o}{V_{o,ripple}} \tag{31}$$

V. Experimental Results

The prototype circuit is applied in the laboratory to demonstrate the performance of the proposed converter. Electrical specifications and circuit components are set as follows:

- Input voltage V_{rms} = 90 V to 264 V (V_m = 127 V to 373 V)
- Output voltage V_o = 100 V
- Line frequency f_1 = 60 Hz
- Switching frequency f_s = 50 kHz
- Output power P_o = 20 W to 100 W (R = 100 Ω to 500 Ω)
- Transformer T_r: n = 0.5 (60 turns:30 turns), core ETD－49, L_m = 850 μH
- Input filter L_f = 3.6 mH and C_f = 330 nF
- Switch S_1: IXFR34N80
- Diode D_o: DSEC30－04A

The voltage gain M is varied from 0.27 to 0.79 according to the electrical specifications. Substituting M = 0.79 and n = 0.5 into (22), the maximum duty ratio D_{max} is derived as 0.61. Substituting D_{max} = 0.61 into (23), τ_{L1B} is obtained as 0.038. Using (24), the inductor L_1 is given by

$$L_1 < \frac{R}{f_s}\tau_{L1B} = \frac{100}{50\text{k}} \times 0.038 = 76\ \mu\text{H}$$

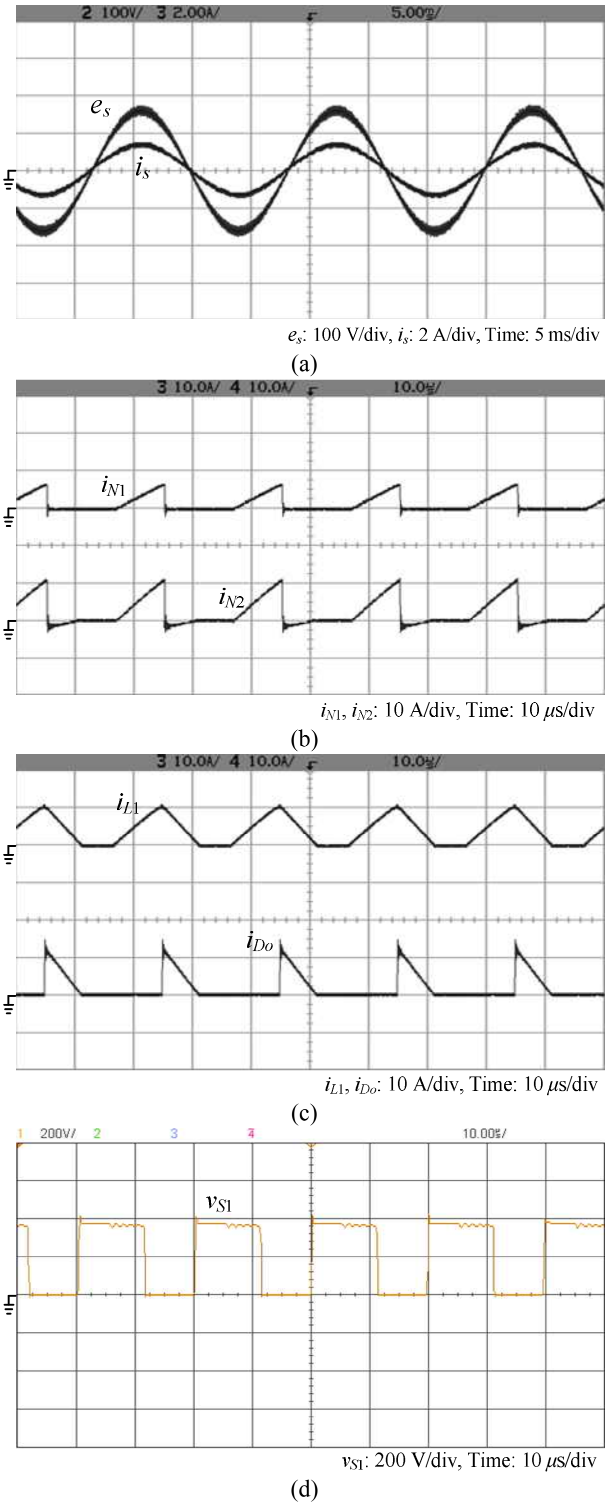

Fig. 9. Experimental waveforms at 115–V_{rms} line voltage: (a) e_s and i_s, (b) i_{N1} and i_{N2}, (c) i_{L1} and i_{Do}, (d) v_{S1}.

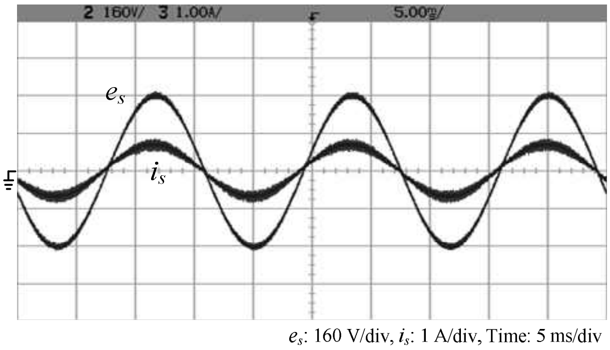

(a)

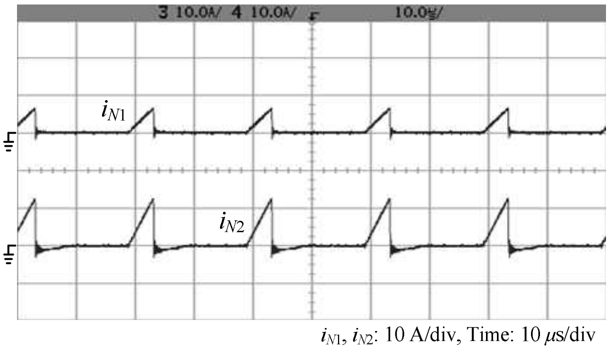

(b)

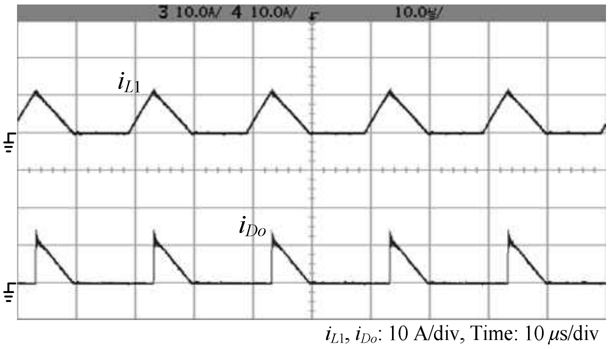

(c)

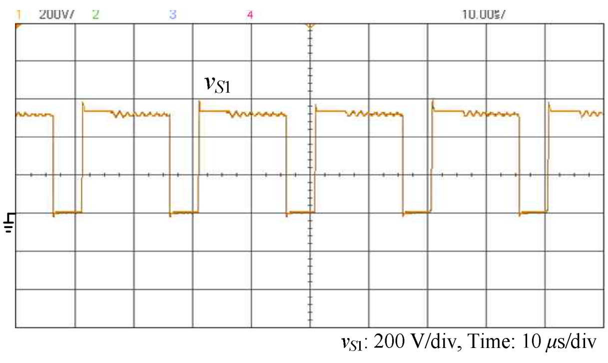

(d)

Fig. 10. Experimental waveforms at 230 - V_{rms} line voltage: (a) e_s and i_s, (b) i_{N1} and i_{N2}, (c) i_{L1} and i_{Do}, (d) v_{S1}

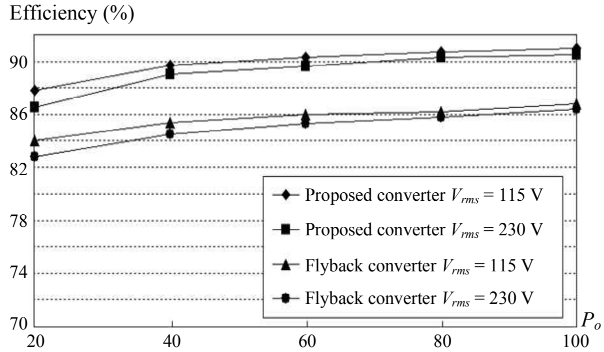

Fig. 11. Measured efficiency for the proposed converter and conventional flyback converter.

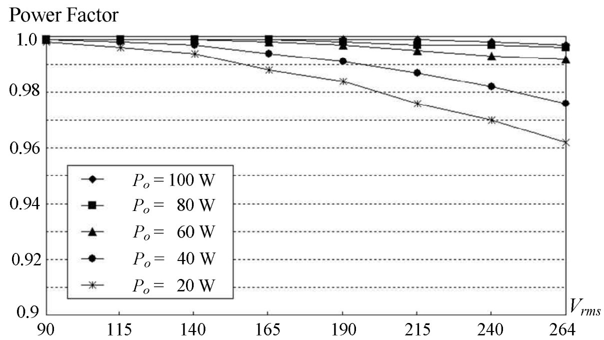

(a)

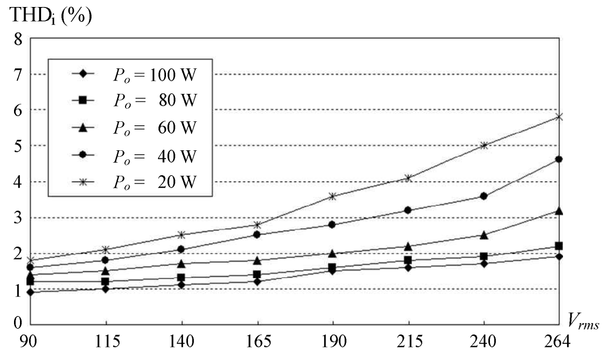

(b)

Fig. 12. Measured results: (a) power factor and (b) THD$_i$.

The inductor L_1 is 60 μH, and the core is EI-40. Thus, τ_{L1} is equal to 0.03 at full load R = 100 Ω and is equal to 0.006 at light load R = 500 Ω. Substituting the two values of τ_{L1} and n = 0.5 into (20), the operating area of the experimental prototype is shown in Fig. 7. The proposed converter is operating in DCM.

Under the operating conditions V_{rms} = 90 V and R = 100 Ω, M and τ_{L1} are derived as 0.79 and 0.03, respectively. Substituting M = 0.79, n = 0.5, and τ_{L1} = 0.03 into (20), duty ratio D is obtained as 0.55. The ripple percentage of V_o is selected as 5%. From (31), the output capacitor inequality is given by

$$C_o \geq \frac{n^2 D^2}{4\omega L_1 f_s M^2} \times \frac{V_o}{V_{o,ripple}} = 536\ \mu\text{F}$$

Thus, output capacitor C_o is selected as 600 μF.

The control circuit is shown in Fig. 8. Figs. 9 and 10 show the experimental waveforms under V_{rms} = 115 V, V_o = 100 V, P_o = 100 W and V_{rms} = 230 V, V_o = 100 V, P_o = 100 W, respectively. In Figs. 9(a) and 10(a), we observe that input current is sinusoidal and is in phase with input voltage. The current waveforms of the transformer primary and secondary sides i_{N1} and i_{N2} are shown in Figs. 9(b) and 10(b), respectively. The waveforms are taken at the peak value of input voltage. The current i_{N2} drops to zero during each switching period, which indicates that the transformer residual magnetism is released to empty during each switching period. The currents i_{L1} and i_{Do} are shown in Fig. 9(c) and 10(c), respectively. We observe that the proposed converter is operated in DCM. The waveform v_{S1} across the switch drain source is shown in Figs. 9(d) and 10(d). The measured efficiencies of the proposed converter and flyback converter are compared in Fig. 11. We observe that efficiency is improved in the proposed converter. The measured power factor and THD_i are shown in Fig. 12. The measured power factor is higher than 0.96, whereas the measured THD_i is lower than 5.8%.

VI. CONCLUSIONS

The forward and flyback PFC AC–DC converters are efficient choices for electrical isolation because of their simple structure. However, the forward AC–DC converter cannot achieve high power factor and low THD_i. Additionally, this converter requires a third winding to recycle transformer magnetizing inductor energy. The flyback AC–DC converter can achieve high power factor and low THD_i. Nevertheless, the transformer leakage inductor results in low efficiency. Therefore, we present a single-phase AC–DC converter that has a simple structure and is operated in DCM to achieve high power factor and low THD_i. A steady-state analysis is conducted. We implement a hardware circuit with simple control logic in the laboratory. The experimental results reveal the performance of the converters. The measured efficiencies reveal that the proposed converter exhibited higher efficiency than the conventional flyback converter.

ACKNOWLEDGMENT

The authors gratefully acknowledge the financial support from the National Science Council of Taiwan under project NSC 102-2221-E-269-010.

REFERENCES

[1] F. Tahami, S. Poshtkouhi, and H. M. Ahmadian, "Piecewise affine control design for power factor correction rectifiers," *Journal of Power Electronics*, Vol. 11, No. 3, pp. 327-334, May 2011.
[2] K. Yao, X. Ruan, X. Mao, and Z. Ye, "Reducing storage capacitor of a DCM boost PFC converter," *IEEE Trans. Power Electron.*, Vol. 27, No. 1, pp. 151-160, Jan. 2012.
[3] J. M. Wang, S. T. Wu, Y. Jiang, and H. J. Chiu, "A dual-mode controller for the boost PFC converter," *IEEE Trans. Ind. Electron.*, Vol. 58, No. 1, pp. 369-372, Jan. 2011.
[4] Y. C. Kimy, L. Jin, J. Lee, and J. Choi, "Direct digital control of single-phase AC/DC PWM converter system," *Journal of Power Electronics*, Vol. 10, No. 5, pp. 518-527, Sep. 2010.
[5] J. M. Alonso, M. A. D. Costa, and C. Ordiz, "Integrated buck-flyback converter as a high-power-factor off-line power supply," *IEEE Trans. Ind. Electron.*, Vol. 55, No. 3, pp. 1090-1100, Mar. 2008.
[6] R. Itoh, K. Ishizaka, H. Oishi, and H. Okada, "Single-phase buck rectifier employing voltage-reversal circuit for sinusoidal input current waveshaping," *IEE Electr. Power Appl.,* Vol. 146, No. 6, pp. 707-712, Nov. 1999.
[7] Y. Jang and M. M. Jovanovic, "Bridgeless high-power-factor buck converter," *IEEE Trans. Power Electron.*, Vol. 26, No. 2, pp. 602-611, Feb. 2011.
[8] H. L. Cheng, Y. C. Hsieh, and C. S. Lin, "A novel single stage high-power-factor AC/DC converter featuring high circuit efficiency," *IEEE Trans. Ind. Electron.*, Vol. 58, No. 2, pp. 524-532, Feb. 2011.
[9] G. K. Andersen and F. Blaabjerg, "Current programmed control of a single-phase two-switch buck-boost power factor correction circuit," *IEEE Trans. Ind. Electron.*, Vol. 53, No. 1, pp. 263-271, Feb. 2006.
[10] J. M. Alonso, J. Vina, D. G. Vaquero, G. Martinez, and R. Osorio, "Analysis and design of the integrated double buck-boost converter as a high-power-factor driver for power-LED lamps," *IEEE Trans. Ind. Electron.*, Vol. 59, No. 4, pp. 1689-1697, Apr. 2012.
[11] A. A. Fardoun, E. H. Ismail, A. J. Sabzali, and M. A. Al-Saffar, "New efficient bridgeless Cuk rectifiers for PFC applications," *IEEE Trans. Power Electron.*, Vol. 27, No. 7, pp. 3292-3301, Jul. 2012.
[12] E. H. Ismail, "Bridgeless SEPIC rectifier with unity power factor and reduced conduction losses," *IEEE Trans. Ind. Electron.*, Vol. 56, No. 4, pp. 1147-1157, Apr. 2009.
[13] M. Mahdavi and H. Farzanehfard, "Bridgeless SEPIC PFC rectifier with reduced components and conduction losses," *IEEE Trans. Ind. Electron.*, Vol. 58, No. 9, pp. 4153-4160, Sep. 2011.
[14] H. Zhang, Y. Zhang, and X. Ma, "Distortion behavior analysis of general pulse-width modulated zeta PFC converter operating in continuous conduction mode," *IEEE Trans. Power Electron.*, Vol. 27, No. 10, pp. 4212-4223, Oct. 2012.
[15] L. K. Chang and H. F. Liu, "A novel forward AC/DC converter with input current shaping and fast output voltage regulation via reset winding," *IEEE Trans. Ind. Electron.*, Vol. 52, No. 1, pp. 125-131, Feb. 2005.
[16] M. Nagao, "A novel one-stage forward-type power factor correction circuit," *IEEE Trans. Power Electron.*, Vol. 15, No. 1, pp. 103-110, Jan. 2000.
[17] M. Daniele, P. K. Jain, and G. Joos, "A single-stage power factor corrected AC/DC converter," *IEEE Trans. Power Electron.*, Vol. 14, No. 6, pp. 1046-1055, Nov. 1999.
[18] B. Singh and G. D. Chaturvedi, "Analysis, design and development of a single switch Flyback buck-boost AC-DC converter for low power battery charging applications," *Journal of Power Electronics*, Vol. 7, No. 4, pp. 318-327, 2007.

[19] J. Zhang, D. D. C. Lu, and T. Sun, "Flyback-based single stage power-factor-correction scheme with time-multiplexing control," *IEEE Trans. Ind. Electron*., Vol. 57, No. 3, pp. 1041-1049, Mar. 2010.
[20] A. Lazaro, A. Barrado, M. Sanz, V. Salas, and E. Olias, "New power factor correction AC-DC converter with reduced storage capacitor voltage," *IEEE Trans. Ind. Electron*., Vol. 54, No. 1, pp. 384-397, Feb. 2007.
[21] K. W. Siu and Y. S. Lee, "A novel high-efficiency flyback power-factor-correction circuit with regenerative clamping and soft switching," *IEEE Trans. Circuits Syst. I, Fundam. Theory Appl.*, Vol. 47, No. 3, pp. 350-356, Mar. 2000.
[22] N. P. Papanikolaou and E. C. Tatakis, "Active voltage clamp in flyback converters operating in CCM mode under wide load variation," *IEEE Trans. Ind. Electron*., Vol. 51, No. 3, pp. 632-640, Jun. 2004.

Chia-Ching Lin was born in Taiwan, R.O.C., in 1959. He graduated from the Department of Electrical Engineering , Far East University, in 1980. He received his M.S. degree in Electrical Engineering from National Cheng-Kung University in 2006. He is currently with the Department of Electrical Engineering, Far East University, Tainan, where he is an Assistant Professor. His research interests are power factor correction and dc-dc converters.

Lung-Sheng Yang was born in Taiwan, R.O.C., in 1967. He received his B.S. degree in Electrical Engineering from National Taiwan Institute of Technology, Taiwan, his M.S. degree in Electrical Engineering from National Tsing-Hua University, Taiwan, and his Ph.D degree in Electrical Engineering from National Cheng-Kung University in 1990, 1992, and 2007, respectively. He is currently with the Department of Electrical Engineering, Far East University, Tainan, where he is an Assistant Professor. His research interests are power factor correction, dc-dc converters, renewable energy conversion, and electronic ballasts.

Ren-Jun Zheng was born in Taiwan, R.O.C., in 1987. He received his B.S. and M.S. degrees from the , and 2007, respectively. He is currently with the Department of Electrical Engineering, Far East University, in 2011 and 2013, respectively. His research interests include power factor correction converter and electronic ballasts.